Mathematical model of dopamine autoreceptors and uptake inhibitors and their influence on tonic and phasic dopamine signaling

Jakob Kisbye Dreyer and Jørn Hounsgaard

J Neurophysiol 109:171-182, 2013. First published 10 October 2012; doi:10.1152/jn.00502.2012

J Neurophysiol 109: 171–182, 2013.
First published October 10, 2012; doi:10.1152/jn.00502.2012.

Mathematical model of dopamine autoreceptors and uptake inhibitors and their influence on tonic and phasic dopamine signaling

Jakob Kisbye Dreyer and Jørn Hounsgaard
Department of Neuroscience and Pharmacology, University of Copenhagen, Copenhagen, Denmark

Submitted 11 June 2012; accepted in final form 4 October 2012

Dreyer JK, Hounsgaard J. Mathematical model of dopamine autoreceptors and uptake inhibitors and their influence on tonic and phasic dopamine signaling. *J Neurophysiol* 109: 171–182, 2013. First published October 10, 2012; doi:10.1152/jn.00502.2012.—Dopamine (DA) D2-like autoreceptors are an important component of the DA system, but their influence on postsynaptic DA signaling is not well understood. They are, directly or indirectly, involved in drug abuse and in treatment of schizophrenia and attention deficit hyperactive disorder: DA autoreceptors influence the behavioral effect of cocaine and methylphenidate and may be the target of antipsychotic medications such as haloperidol. DA autoreceptors are active at two levels: Somatodendritic autoreceptors mainly influence firing rate of DA neurons, and presynaptic autoreceptors control release of neurotransmitter at axonal terminals. Here we develop a mathematical model that captures the dynamics of this dual autoregulation system. Our model predicts a biphasic autoreceptor response between DA terminals and somatodendritic regions that influences the postsynaptic integration of DAergic firing patterns. We applied our model to study how DA uptake inhibition affects the translation of DA cell firing into activation of postsynaptic DA receptors. While uptake inhibition increased tonic activation of low-affinity postsynaptic receptors, high-affinity state receptors saturated and thus became insensitive to phasic DA signaling. This effect had remarkable regional specificity: While high-affinity DA receptors saturated at low levels of uptake inhibition in nucleus accumbens, they only saturated at higher levels of uptake inhibition in dorsal striatum. Based on high-affinity receptor saturation, the model predicted that removal of autoreceptor control would lead to cocaine hypersensitivity.

burst; striatum; nucleus accumbens; D2 receptor; D1 receptor; cocaine; methylphenidate; D2 antagonist; D2 agonist; locomotor; ADHD; reward; antipsychotic; modeling; computational analysis

DOPAMINE (DA) in nucleus accumbens (NAcc) and dorsal striatum (DS) is critical for reward- and goal-oriented behavior (Grace et al. 2007; Schultz 1998). DA signaling, or the lack thereof, is the turning point of major disorders such as drug abuse, schizophrenia, Parkinson's disease, and attention deficit hyperactive disorder (ADHD) (Dagher and Robbins 2009; Howes and Kapur 2009; Volkow et al. 2011).

A wide range of DA-related behavior and cognitive functions are distorted by either too low or too high DA levels (Cools and D'Esposito 2011). Thus precise control over the DA signal seems highly critical to normal function. For this reason it is no surprise that DA neurons are controlled by a complex system of D2 and D3 autoreceptors. Reduced autoreceptor control has been implicated in impulsivity (Buckholtz et al. 2010) and enhances the behavioral effect of cocaine (Bello et al. 2011). DA autoreceptors may even be a primary target of certain antipsychotics (Moller 2005).

DA autoreceptors affect multiple aspects of DA signaling including firing rate, DA synthesis, and terminal release (Beaulieu and Gainetdinov 2011). DA release in somatodendritic regions interacts with somatodendritic autoreceptors inhibiting firing of DA neurons (Beckstead et al. 2004; Cragg and Greenfield 1997; Pucak and Grace 1994). At the same time, DA release from axonal terminals interacts with D2 receptors expressed on presynaptic terminals regulating release and synthesis (Benoit-Marand et al. 2001; Dugast et al. 1997; el Mestikawy et al. 1986; Schmitz et al. 2003).

The rich dynamics of DA autoreceptors and their influence on DA levels and transients has been studied intensively (Benoit-Marand et al. 2001; Gonon and Buda 1985; Phillips et al. 2002; Zhang et al. 2009). However, a unified description of the coupling between pre- and postsynaptic DA signaling is still lacking. Fixed-amplitude models neglect dynamic changes in DA release (Dreyer et al. 2010; Venton et al. 2003; Wightman and Zimmerman 1990). Consequently, they are only valid for small perturbations in DA signaling. Variable-release models include facilitation and depression of release by artificially evoked spike trains (Montague et al. 2004). However, the static parameters of the variable-release model include implicit effects of multiple factors including autoreceptors, uptake, diffusion, and tonic DA activity. Thus the dynamic changes in DA signaling when the relative contributions of these factors are altered by drugs or disease are not accounted for.

Here we model how somatodendritic and presynaptic autoreceptors influence activation of postsynaptic DA D1 and D2 receptors by DA cell firing. In our model, the contribution of autoreceptors is explicit so that effects of their manipulations can be estimated and tested. Reliable estimates of concurrent pre- and postsynaptic DA transmission required a bottom-up biophysical reconstruction of DA release in axonal terminal fields, including estimates of the occupancy of terminal autoreceptors. At the same time, concurrent somatodendritic release was simulated to provide negative feedback for the firing of DA neurons.

In the first part of this report we provide estimates of DA levels and transients and make predictions on how these may be altered in typical experimental paradigms in which DA release is evoked by electrical stimulations. We found that autoreceptors introduce an interplay between somatodendritic and terminal DA.

We then investigate how autoreceptors influence postsynaptic signaling of naturally occurring phasic firing patterns relevant for reward signaling (Schultz 1998). We found that high- and low-affinity postsynaptic receptors were differentially af-

Address for reprint requests and other correspondence: J. K. Dreyer, Dept. of Neuroscience and Pharmacology, Univ. of Copenhagen, Blegdamsvej 3, 2200 Copenhagen, Denmark (e-mail: jakobdr@sund.ku.dk).

fected by bursts and pauses in DA cell firing. Autoreceptors effectively increased the specificity of burst and pauses to low- and high-affinity postsynaptic receptors.

Finally, we apply the model to study the effect of DA uptake inhibition on the translation of DA cell firing to activation of postsynaptic receptors. Here, the most prominent effect of uptake inhibition was saturation of high-affinity postsynaptic receptors. This blocked their ability to respond to phasic DA cell firing. In NAcc this occurred at levels of uptake inhibition in the therapeutic range, whereas DS was affected by uptake inhibition at locomotor-stimulating levels.

Glossary

ADHD	Attention deficit hyperactive disorder
$AR(\mathbf{r},t)$	Occupancy at time t of autoreceptors at location $\mathbf{r}$
$AR_j^i(t)$	Average occupancy of autoreceptors at terminal i on neuron j
AUC	Area under curve
C	Concentration of dopamine
DA	Dopamine
DAT	Dopamine transporter
ΔC_{soma}	Incremental release of somatodendritic DA for a single action potential
D_{coc}^{ip}	Dose of ip cocaine (mg/kg)
D_{coc}^{iv}	Dose of iv cocaine (mg/kg)
DRH	High-affinity postsynaptic dopamine receptor (EC_{50} = 0.010 μM)
DRL	Low-affinity postsynaptic dopamine receptor (EC_{50} = 1 μM)
DS	Dorsal striatum
ip	Intraperitoneal
iv	Intravenous
k_{off}	Off-rate for DA binding to presynaptic autoreceptors
k_{on}	On-rate for DA binding to presynaptic autoreceptors
K_{app}	Apparent Michaelis-Menten constant
K_i	Inhibition constant for competive uptake inhibitor
K_m	Michaelis-Menten constant
MP	Methylphenidate
NAcc	Nucleus accumbens
ν_{eff}	Effective firing rate of DA neurons, realized by input firing rate minus inhibition by somatodendritic autoreceptors
ν_{in}	Input firing rate to the model; the firing rate realized in absence of somatodendritic autoinhibition
P_{max}	Highest possible vesicular release probability
P_{min}	Lowest possible vesicular release probability
P_r	Vesicular release probability
SNc	Substantia nigra pars compacta
V_{max}	Michaelis-Menten uptake parameter
VTA	Ventral tegmental area

METHODS

The aim of this work was to develop an integrated model of DA volume transmission that can predict the dynamic effects of somatodendritic and presynaptic DA autoreceptors and how these influence the postsynaptic effect of DA cell firing. The input parameters to the model are primarily based on observations in rodents.

We analyzed DA signaling from a systems perspective and investigated volume-mediated signals by an ensemble of DA neurons projecting to a common target area in NAcc or DS (Dreyer et al. 2010). We assumed that the activity of the ensemble was described by the population-averaged firing rate. The experimentally observed firing rate is determined by a combination of external synaptic input and intrinsic currents where inhibitory GIRK channels controlled by somatodendritic autoreceptors play a partial role. In our systems approach we separated these terms so that

$$\nu_{eff} = \nu_{in} - \Delta\nu_{auto} \quad (1)$$

Here ν_{eff} is the effective firing rate and ν_{in} is the input firing rate. The effective firing rate is the firing rate observed experimentally and determines both somatodendritic and terminal release. The input firing rate is defined as the firing rate of DA neurons driven by all external and internal current inputs except those mediated by autoreceptors. The last term, $\Delta\nu_{auto}$, is the reduction in firing rate mediated by currents induced by somatodendritic autoinhibition.

To keep matters simple, we avoided direct calculation of the ionic currents assumed to be responsible for these terms. Instead, we established an empirical relation between DA levels in the somatodendritic region directly and the effective firing rate based on experimental data (see Fig. 1 and *Eq. 5*).

Similarly, we assumed terminal release probability to be regulated by the occupancy of presynaptic autoreceptors. These autoreceptors are assumed to be sensitive to the local DA level around release sites. Again we established a heuristic relation between occupancy of presynaptic autoreceptors at a given terminal and its release probability but avoided direct calculation of the underlying ionic currents at the terminal assumed to mediate the effect.

Consequently, the dual autoregulation system was modeled as two systems, somatodendritic and terminal, each providing a feedback mechanism based on the local DA concentration. Finally, activation of postsynaptic DA receptors was predicted from the spatiotemporal concentration of extracellular DA in terminal areas assuming DA volume transmission (Dreyer et al. 2010). When applying the model to investigate the effect of uptake inhibition we assumed that these directly increased the apparent Michaelis-Menten constant (K_{app}) of the uptake.

Implementation of competitive uptake inhibition. When simulating inhibited uptake conditions we used a $K_{app} \geq K_M$, where $K_M = 0.16$ μM is the native uptake constant (John and Jones 2007). To bridge with in vivo studies, we assumed the following linear relation between intraperitoneal (ip) dose of cocaine and apparent uptake constant:

$$K_{app} = 0.056\ \mu\text{M(mg/kg)}^{-1} D_{coc}^{ip} + K_M \quad (2)$$

where D_{coc}^{ip} is the ip dose of cocaine in milligrams per kilogram. *Equation 2* is based on the observation by Oleson et al. (2009) that K_{app} peaks at 1.0062 μM after administration of 15 mg/kg ip cocaine. Note that this value of K_{app} is reached 20 min after delivery of drug (Oleson et al. 2009). We also use *Eq. 2* when discussing uptake inhibited by ip methylphenidate (MP). In this case, we correct for the different inhibitory potency at the dopamine transporter (DAT) (K_i = 0.35 μM for cocaine and K_i = 0.21 μM for MP; John and Jones 2007). Relative scales between K_{app} and doses of ip cocaine and ip MP are provided on the *x*-axis of Fig. 1*A*. Under these assumptions, 2 mg/kg ip MP or 3 mg/kg ip cocaine blocks ~50% of the DAT, and we consider this to be the therapeutically relevant level of DAT inhibition (Volkow et al. 1998).

To estimate apparent uptake constants after intravenous (iv) cocaine, we interpolated linearly over the peak values in experimentally observed K_{app} by España et al. (2008). The resulting relation was

$$K_{app} = 0.80\ \mu\text{M(mg/kg)}^{-1} D_{coc}^{iv} + K_M \quad (3)$$

Note that for iv administration the peak value occurs within 30–60 s after delivery of drug (Espana et al. 2008).

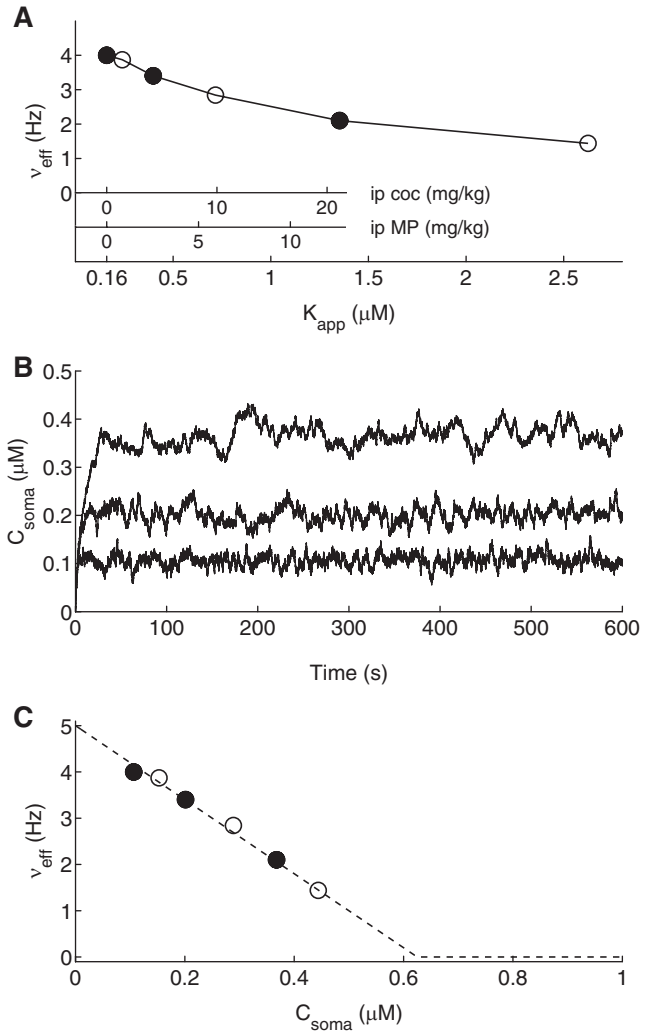

Fig. 1. Construction of somatodendritic autoreceptor feedback. *A*: firing rates (ν_{eff}) from Einhorn et al. (1988) plotted against estimated apparent uptake constant (K_{app}) with *Eq. 3*. Firing rate was put on an absolute scale assuming 4-Hz firing rate in the control case. Filled markers indicate the 3 conditions plotted in *B*. *B*: concentration of somatodendritic dopamine (DA) (C_{soma}) using the combination of firing rate and K_{app} shown in *A*. The 3 conditions correspond to ν_{eff} = 4 Hz and K_{app} = 0.16 μM (*bottom*), ν_{eff} = 3.4 Hz and K_{app} = 0.40 μM (*middle*), and ν_{eff} = 2.1 Hz and K_{app} = 1.35 μM (*top*). *C*: Einhorn firing rate plotted against numerically determined somatodendritic DA levels. Filled markers indicate the conditions shown in *B*. Dashed line, ν_{eff} as given by *Eq. 5*.

Our simulations assume steady-state concentrations of inhibitor on a timescale of 1 min that approximate ip administration better than iv adminstration. We will therefore use *Eq. 2* except where noted.

Since we assume constant levels of uptake inhibitor, our results are mostly relevant for therapeutic applications, where MP is a typical drug. However, many animal studies use ip cocaine as a model substance. Therefore we will compare our computational results with empirical results of either cocaine or MP where appropriate.

Determination of effective DAergic firing rate and somatodendritic DA concentration. The effective firing rate is determined from the input firing rate and somatodendritic autoinhibition depending on the somatodendritic DA concentration.

Thus we needed to calculate somatodendritic DA levels in our model. Experimentally the spike amplitude of DA release in somatodendritic regions is modulated very little by autoreceptors (Cragg and Greenfield 1997). For simplicity we therefore used a fixed-amplitude model to calculate the somatodendritic DA level as a function of the effective firing rate (Wightman and Zimmerman 1990). The somatodendritic DA concentration, C, was determined numerically by solving

$$\frac{dC_{soma}}{dt} = \Delta C_{soma}\Pi_{spike}(\nu_{eff}) - \frac{V_{max}^{soma}C_{soma}}{K_{app} + C_{soma}} \quad (4)$$

where ΔC_{soma} = 0.02 μM is the incremental release of DA per spike, V_{max}^{soma} = 0.2 μM/s is the maximum DA uptake capacity in the somatodendritic region (John et al. 2006), and Π_{spike} is a stochastic variable taking value 1 if a spike occurs within the current time step of the integration and 0 otherwise. This was determined by a Poisson process depending on the effective firing rate ν_{eff}. To minimize the effect of random fluctuations we averaged *Eq. 4* 10 times to calculate C_{soma}.

To model somatodendritic autoreceptors we needed to determine the link between somatodendritic DA levels and how this reduces effective firing rate. For this we used the relation between tonic firing rate and iv dose of cocaine established by Einhorn et al. (1988). We first assumed that ν_{eff} = 4 Hz in the control case and linked effective firing rate and K_{app} calculated with *Eq. 3* (Fig. 1*A*; each data point corresponds to an observation by Einhorn et al., and filled markers indicate conditions shown in Fig. 1*B*). We then used *Eq. 4* to calculate somatic DA levels for each pair of ν_{eff} and K_{app} (Fig. 1*B*). We then observed a linear relation between the average DA levels and effective firing rate (Fig. 1*C*; circles correspond to Einhorn et al. observations, filled markers are the conditions shown in Fig. 1*B*, and dashed line is the linear relation ν_{eff} = 5 Hz − 8 Hz/μM × C_{soma}).

We assumed this linear relationship to reflect a fundamental relation between different components affecting firing of DA neurons. We therefore generalized the linear relation and assumed that autoreceptors reduce cell firing with an amount proportional to somatodendritic DA levels.

Since effective firing rate determines its own inhibition, we constantly updated effective firing rate and somatodendritic DA levels in parallel. In each time step ν_{eff} was determined from the instantaneous somatodendritic DA levels with

$$\nu_{eff}(t) = \begin{cases} \nu_{target}(t) - \alpha C_{soma}(t) & \text{for } \alpha C_{soma}(t) < \nu_{target}(t) \\ 0 & \text{for } \alpha C_{soma}(t) \geq \nu_{target}(t) \end{cases} \quad (5)$$

where α = 8 Hz/μM and ν_{in} indicates the input firing rate. Note that if $\alpha C_{soma} > \nu_{in}$, the effective firing rate is set to 0. We use ν_{in} as control parameter of the model, and bursts and pauses in neuron population are generated by temporal variations in input firing rate.

When simulating artificially evoked release we assumed that the firing rate of the evoked spike train was independent of somatodendritic autoinhibition.

Calculation of extracellular DA level in axon terminal regions. The DA levels in terminal regions were calculated by a diffusion model incorporating DA vesicular release from distinct release sites, extracellular diffusion, and Michaelis-Menten reuptake. Details and parameters are described in Dreyer et al. (2010). In brief, the model describes three-dimensional (3D) spatiotemporal evolution of DA concentration in cubic volume. DA levels in the simulation space were determined by vesicular release from spatially distinct terminals.

By selecting different parameter settings we modeled DA signaling in either NAcc or DS. In our model these two areas differ by innervation density of DA terminals (DS 0.1 terminal/μm^3, NAcc 0.06 terminal/μm^3; Doucet et al. 1986) and by total uptake capacity (DS V_{max} = 4.1 μM/s, NAcc V_{max} = 1.5 μM/s; Cragg and Rice 2004; Garris et al. 1994a). The size of the simulation space was set to accommodate exactly 1,500 DA release sites. Thus the diameter of the simulation space was 29.2 μm when simulating NAcc and 24.7 μm when simulating DS. Figure 2*A* shows a high-spatial-resolution image of instantaneous DA concentrations during tonic firing. Black dots indicate DA release sites, and the spatial concentration of extracellular DA is indicated by color.

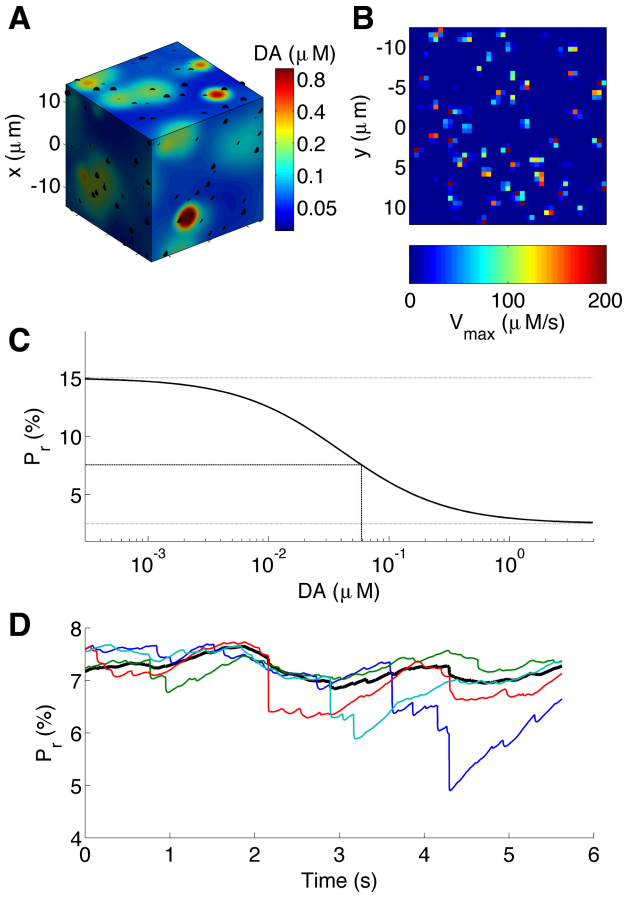

Fig. 2. Construction of terminal DA release and presynaptic autoreceptor feedback. *A*: spatial distribution of DA in terminal simulation space during tonic firing. Color indicates extracellular concentration of DA as indicated on the color bar. Black dots indicate DA release sites. Note that the volume is filled with 1,500 DA release sites and only those close to the boundary are visible on this plot. To better illustrate 3-dimensional heterogeneity of DA concentration, the image has higher spatial resolution than during typical simulations. *B*: distribution of DA uptake capacity in a section through the simulation space in the *y*-*z* plane. Color indicates uptake capacity (V_{max}). The spatial resolution is as in typical simulations. *C*: relation between equilibrium DA levels and release probability (P_r). Dashed black line shows the resting value of P_r and baseline DA levels under 4-Hz tonic firing. *D*: P_r of different terminals. Black line indicates average.

Because of anatomical constraints, the terminal simulation space is assumed to contain terminals from an ensemble of 100 different neurons. Spikes of each neuron were determined by independent Poisson processes with intensity determined by ν_{eff}. Thus the average firing rate across the ensemble was approximately ν_{eff} but with fluctuations due to the random spike generating process. The Poisson process was also used when simulating evoked release.

To accurately model the location of DAT at terminals, we focused DA uptake at the release sites (Fig. 2*B*; spatial resolution as in typical simulations). Details concerning the implementation of localized DA uptake are given below.

Autoreceptor control of terminal release probability. Experimental voltammetry studies show that autoreceptor control of axonal terminal DA release is bidirectional: Release is increased by D2 antagonist drugs and decreased by D2 agonists. Typically the dynamic range observed roughly covers a factor of 2 to either side in evoked DA release (Dugast et al. 1997; Gonon and Buda 1985; Herr et al. 2010; Wu et al. 2002). In our model, the spike amplitude of terminal DA release is proportional to the density of release sites, the number of DA molecules in DA vesicles, and the probability that a terminal releases a vesicle with an action potential (Dreyer et al. 2010; Wallace and Hughes 2008). Even though DA autoreceptors could potentially be involved in regulation of all of these factors, we find it most likely that the fast timescale effects relevant for phasic DA signaling are mediated by dynamic modulation of the release probability.

In our model, terminal i on neuron j releases a vesicle with probability P_j^i when neuron j fires. In a preliminary study we estimated the typical vesicular release probability to be 6% (Dreyer et al. 2010). To be consistent with the approximately twofold dynamic range of release amplitudes we therefore set $P_{min} = 2.5\%$ as the minimal release probability, corresponding to terminal autoreceptors fully activated, and $P_{max} = 15\%$ as the maximal release probability, realized when terminal autoreceptors are fully deactivated. To enable bidirectional control we assumed the EC_{50} of terminal autoreceptors to be 40 nM, around the expected basal level of the model (Dreyer et al. 2010).

Occupancy and spatial distribution of presynaptic autoreceptors. We assumed that the release probability per action potential for each release site was controlled by autoreceptors sensitive to the time-varying DA level around the terminal. The occupancy of autoreceptors at location $\mathbf{r}$ at time t was calculated dynamically by numerical integration of

$$\frac{\mathrm{dAR}(\mathbf{r},t)}{\mathrm{d}t} = C(\mathbf{r},t)k_{on}\big(1 - \mathrm{AR}(\mathbf{r},t)\big) - k_{off}\mathrm{AR}(\mathbf{r},t) \qquad (6)$$

where $C(\mathbf{r},t)$ is the concentration of DA at position $\mathbf{r}$ and at time t, $\mathrm{AR}(\mathbf{r},t)$ is the corresponding occupancy of autoreceptors, and k_{off} and k_{on} denote the off- and on-rates of DA interaction with terminal D2 receptors. To our knowledge, these on- and off-rates have not been directly measured for DA. We used $k_{on} = 10\ \mu\mathrm{M}^{-1}\mathrm{s}^{-1}$ (Chance 1943) and set $k_{off} = 0.4\ \mathrm{s}^{-1}$ to give 50% occupancy at the EC_{50} described above. We verified that the time course of autoinhibition was in agreement with experimental observations (Benoit-Marand et al. 2001; Phillips et al. 2002).

Equation 6 describes the occupancy state of autoreceptors at any location in simulation space. The influence of autoreceptors on a particular terminal was determined as a weighted average of $\mathrm{AR}(\mathbf{r},t)$ where autoreceptors close to the terminal have the highest influence. Thus for terminal i on neuron j the average occupancy of terminal autoreceptors at time t was determined as

$$\mathrm{AR}_i^j(t) = \int_\Omega \frac{\mathrm{AR}(\mathbf{r},t)}{\left(2\pi r_{term}^2\right)^{3/2}} \exp\left(\frac{\left(\mathbf{r} - \mathbf{r}_{ij}\right)^2}{2r_{term}^2}\right)\mathrm{d}\mathbf{r} \qquad (7)$$

where $r_{term} = 0.25\ \mu$m is the half-width of the terminal (Pickel et al. 1992) and $\mathbf{r}_{ij}$ is the location of the terminal. The integral extends over the simulation space, and the normalization was corrected for boundary effects.

Once the average occupancy of terminal autoreceptors for the terminal was established, the release probability was determined by linear interpolation

$$P_i^j(t) = (P_{min} - P_{max})\mathrm{AR}_i^j(t) + P_{max} \qquad (8)$$

where $P_{min} = 2.5\%$ and $P_{max} = 15\%$ as described above (Fig. 2*C* shows relationship between equilibrium DA concentration and P_r). Note that the release probability describes the probability of release for a single terminal, number i on neuron j. Different terminals in the simulation space will generally experience different dynamical DA concentrations and therefore have different release probabilities. In particular, a single vesicular release event will briefly reduce the release probability of the releasing terminal in a time span after the release (Fig. 2*D*; see red line at time = 2.2 s and blue line at time = 4.3 s).

Presynaptic location of dopamine transporters. Since DAT are primarily expressed on DA neurons near release sites (Hersch et al. 1997), we used a space-dependent uptake,

$$V_{max}(\mathbf{r}) = \sum_{ij} \frac{V_0}{\left(2\pi r_{term}^2\right)^{3/2}} \exp\left(\frac{\left(\mathbf{r} - \mathbf{r}_{ij}\right)^2}{2r_{term}^2}\right) \quad (9)$$

where V_0 is a constant equivalent to the uptake capacity per terminal; other parameters are defined as in *Eq. 7*. The value of V_0 was selected so that the total volume-averaged uptake was equal to V_{max} in the simulation space, such as 1.5 μM/s for simulation of NAcc. In *Eq. 9* the uptake capacity is high near release sites and low further away, as shown in Fig. 2*B*.

Electrochemical measurements of DA uptake typically use carbon ~50 μm long (Venton et al. 2003). Such electrodes sample volumes considerably larger than 1 μm^3 and therefore report the volume average of $V_{max}(\mathbf{r})$. In our simulations the DA levels and activation of pre- and postsynaptic receptors were also mainly determined by the volume-averaged uptake (see below).

Quantification of postsynaptic DA signaling. Postsynaptic DA receptors are classified as D1-like or D2-like receptors depending on their ability to facilitate or depress the production of postsynaptic cyclic AMP (Beaulieu and Gainetdinov 2011). Both of these receptor subtypes may exist in high- and low-affinity states. We hypothesized spatially uniform distributions of low-affinity (DRL, $EC_{50} \approx 1{,}000$ nM) and high-affinity (DRH, $EC_{50} \approx 10$ nM) receptors (May 1992) and assumed these receptors to be sensitive to DA volume transmission in terminal areas. In each time step of the simulation, the activity of postsynaptic DA receptors was determined as a 3D volume integral of the spatial distribution of terminal DA (Fig. 2*A*) assuming local quasiequilibrium (Dreyer et al. 2010).

The effect of bursts or pauses was quantified in terms of the change in area under the curve (ΔAUC), calculated as

$$\Delta AUC = \int_0^T \left(DR_{phasic}(t) - \langle DR_{tonic} \rangle\right) dt \quad (10)$$

where $DR_{phasic}(t)$ is the estimated activation of DA receptor (either high or low affinity) and $\langle DR_{tonic} \rangle$ is the average activation by tonic firing in the same brain region and with the same level of uptake inhibition. Except where stated, the integral extended over the whole duration of the transient, including possible long-term compensatory effects of somatodendritic and terminal autoinhibition. Note that when the phasic signal is a pause, ΔAUC becomes negative.

Bursts and pauses were simulated as a repeating pattern of 4 cycles each with a period of 10 s of simulated time. The initial DA level in the simulation space was estimated by the tonic firing rate, uptake, and autoinhibition. To stabilize DA levels, simulations were run for 5 s of simulated time before results were collected.

The model was implemented in MATLAB 7.8 (MathWorks), and numerical integration was performed with the forward Euler method.

RESULTS

Tonic and phasic activation of terminal autoreceptors. We used our model to investigate DA signaling in DS and NAcc, areas highly innervated by DA terminals.

We first investigated DA levels produced by steady-state tonic firing. By setting $\nu_{in} = 5$ Hz, our model stabilized at ~4 Hz effective firing rate and with constant somatodendritic DA level around 0.1 μM.

The tonic activity gave 0.047 $\pm$ 0.01 μM baseline level in DS and 0.067 $\pm$ 0.01 μM in NAcc (means $\pm$ SD). Here the standard deviation indicates variability due to random fluctuation in firing rate and stochastic release. Considering that critical parameters such as tonic firing rate, DA innervation density, and uptake have high variability even within the same subject, we consider the above difference in tonic DA levels between NAcc and DS to be relatively small compared with the inherent uncertainty in our model (Garris et al. 1994b; Grace and Bunney 1984b; Hyland et al. 2002; Koulchitsky et al. 2012; Moquin and Michael 2009; Wightman et al. 2007).

With tonic activity, the average release probability across terminals was 7–8% (Fig. 2*D*). Comparing with the maximal release probability ($P_{max} = 15\%$), this relative difference indicates a substantial tonic occupancy of terminal autoreceptors as observed by Dugast et al. (1997). In comparison, the difference between input firing rate (5 Hz) and effective firing rate (4 Hz) mediated by tonic DA levels in somatodendritic regions was relatively small. This is in agreement with the 20% increase in firing rate after administration of D2 receptor antagonists observed by Pucak and Grace (1994).

We then investigated the time course of autoinhibition, using evoked transients. Here we simulated two evoked DA transients each generated by evoked release equivalent to 3 spikes at 100-Hz firing rate. The trains were separated by a small time difference Δt. We then determined the amplitude of the second transient relative to the first transient (Fig. 3*A1*). We found that inhibition was maximal at $\Delta t = 200$–400 ms and decayed over 2 s (Fig. 3*A2*). The time course is similar to observations in vivo by Benoit-Marand et al. (2001) (Fig. 3*A2*) and in vitro by Phillips et al. (2002). However, at $\Delta t < 100$ ms our model underestimates the trailing DA transient, probably because it does not include pulse-to-pulse facilitation.

Complex interplay between DA levels in somatodendritic region, firing rate, and terminal release. Our model couples somatic and terminal autoinhibition, two systems with different kinetics and behavior. When the DA system is perturbed from the resting state, for example by strong evoked release, the combined response of these systems may not be easily discerned experimentally. We therefore modeled typical experimental situations where transient release from DA neurons is evoked artificially.

We first investigated the case where tonic firing is interrupted by an evoked 0.5-s stimulus at a 20-Hz firing rate (giving on average 10 spikes per DA neuron). The effective firing rate during the stimulus was assumed to overcome the effect of somatodendritic autoinhibition; only the spontaneous activity after the stimulus was affected.

The stimulus evoked a somatodendritic DA transient of 0.2 μM (Fig. 3*B*) that in turn caused a temporal poststimulus depression in effective firing rate, from 4 Hz before the stimulus to 2.4 Hz after the stimulus. The slow decay of the somatodendritic DA transient led to a relatively slow recovery of the effective firing rate (Fig. 3*C*, *inset*).

In DS we observed a DA transient of ~0.3 μM in amplitude (Fig. 3*D*). The onset of the transient was relatively fast. However, during the stimulus the release was reduced and the transient stagnated. This was mediated by temporal reduction of the release probability at the terminal level (Fig. 3*E*). Thus saturation of terminal autoreceptors affected the shape of the transient.

We then calculated the effective firing rate following a strong stimulus, equivalent to 50 spikes at 60 Hz. Because the stimulus evoked a somatodendritic transient higher than 0.63 μM (Fig. 3*B*), we observed a complete stop in firing ($\nu_{eff} = 0$) lasting 3 s after termination of the stimulus and a depression of firing for up to 10 s after end of the stimulus (Fig. 3*C*, *inset*). This may be compared with experimental observations by Kuhr et al., where electrical stimulation of the medial forebrain

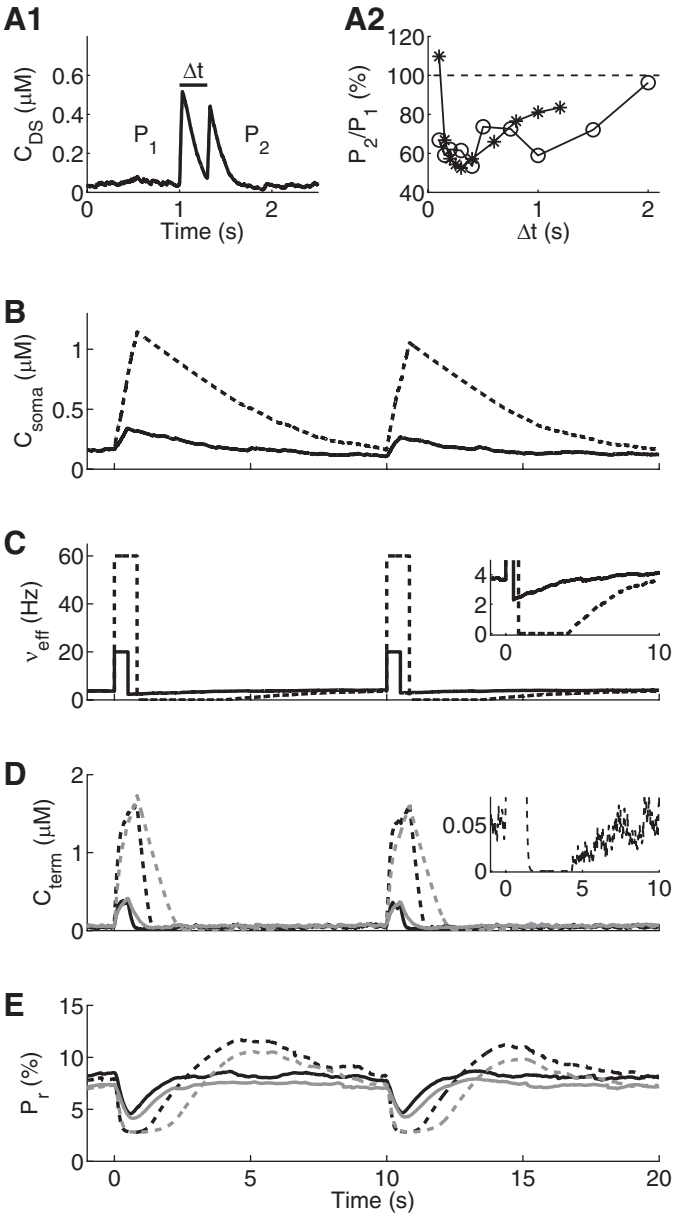

Fig. 3. Analysis of interaction between somatodendritic and terminal autoinhibition with evoked release. *A1*: data from pair pulse simulation. Each transient was evoked by simulating a train of 3 pulses at 100 Hz; each train was separated by Δt. The height of the first transient is denoted P_1 and the height of the second transient P_2. C_{DS}, dorsal striatum DA levels. *A2*: circles, P_2/P_1 as function of Δt; asterisks, experimental data reproduced from Benoit-Marand et al. (2001). In *B–E* dashed lines indicate strong stimulus (50 spikes at 60 Hz), and solid lines indicate light stimulus (10 spikes at 20 Hz). *B*: somatodendritic DA levels from stimulated release and tonic firing rate. Plot shows 2 cycles each of 10 s. *C*: ν_{eff} of DA neurons corresponding to somatic DA levels in *B*. *Inset*: close view of ν_{eff} during 1 stimulus cycle. Note that during stimulated release, ν_{eff} is not affected by autoinhibition. *D*: resulting DA levels in terminal regions (C_{term}). Results are shown for dorsal striatum (DS) in black and for nucleus accumbens (NAcc) in gray. *Inset*: close view of DS DA levels after strong stimulus. *E*: concurrent release probability at the terminal level; same colors as in *D*.

bundle by 120 pulses at 60 Hz caused a 90% reduction of DA cell firing in the first 10 s and a 50% reduction of cell firing between 10 and 20 s after the stimulus (Kuhr et al. 1987).

As a result of the high effective firing rate, we observed a 1.6 μM DA transient in DS. The transient had biphasic shape, with quick onset transiting into a slower increase phase 200–300 ms after onset of stimulus. After the stimulus the concentration of DA reached 0 because of the poststimulus inhibition of firing rate (Fig. 3*D* and *inset*).

The strong stimulus evoked considerable increase in presynaptic autoinhibition. During the 60-Hz stimulus, the release probability came close to the minimum value of 2.5%. Interestingly, after the stimulus ended the long-lasting depression of tonic firing was compensated by a reduction in tonic terminal autoinhibition. Thus 3–8 s after the stimulus terminal release probability was increased compared with the resting value (Fig. 3*E*).

Qualitative differences in autoreceptor control between DS and NAcc are often observed experimentally (Zhang et al. 2009). It is not known whether these differences are mediated directly by different autoreceptor architecture or indirectly, by differences in release and uptake. We therefore compared simulated autoreceptor control of evoked release in NAcc and DS.

DAergic neurons that project to NAcc are located in ventral tegmental area (VTA), whereas DAergic neurons in substantia nigra pars compacta (SNc) project to DS. For simplicity we assumed that somatodendritic DA concentrations could be estimated with the same parameters. Therefore the evoked stimuli in either region shared somatodendritic DA concentration and also the same effective firing rate (Fig. 3, *B* and *C*). The transients produced by the same stimuli were of similar size, but transients in NAcc appeared less bimodal and thus seemed less affected by terminal autoreceptors than those in DS (Fig. 3*D*). However, the temporal evolution of the release probability in the two simulated regions was qualitatively similar (Fig. 3*E*). Thus, in our model, differences in release and uptake account for the different shapes of evoked transients in DS and NAcc.

Autoinhibition allows specific postsynaptic integration of phasic DA signals. Bursts and pauses in firing of midbrain DA neurons are hypothesized to encode reward prediction errors giving crucial information for behavior (Bayer et al. 2007; Schultz 1998). Our model predicts that a brief burst will be followed by a long-lasting somatodendritic depression in firing rate. Also, a pause in cell firing may evoke temporarily increased firing rate after the pause. These effects oppose phasic signals, and, if not carefully balanced, they could possibly quench their postsynaptic integration. We therefore estimated how autoreceptors affected the postsynaptic activation of high-affinity (DRH) and low-affinity (DRL) DA receptors to bursts and pauses.

We represented bursts by tonic activity interrupted by a 21-Hz input firing rate (giving 20-Hz effective firing rate with the amount of autoinhibition generated by tonic somatodendritic DA levels). The bursts were of varying length between 0.05 s and 0.6 s, equivalent to 1–12 spikes at a 20-Hz effective rate.

The effective firing rate during bursts was influenced by somatodendritic DA levels (Fig. 4*A1*). At burst onset, the effective firing rate was close to 20 Hz. Thereafter, the effective firing rate decreased slightly during the burst, and for the longest burst the effective firing rate was 19 Hz at the end (Fig. 4*B1*). After the burst, increased somatodendritic autoinhibition led to lower effective tonic firing rates; after the longest burst the tonic firing rate had dropped to 2.8 Hz (Fig. 4*B1*, *inset*).

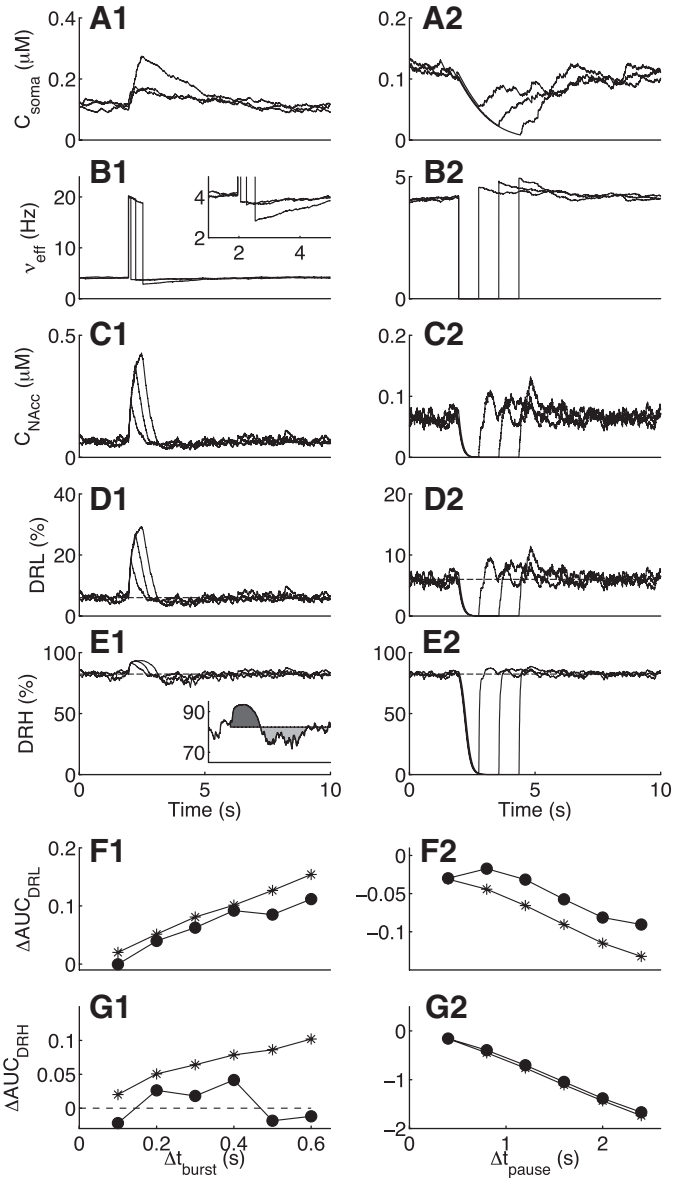

Fig. 4. Autoreceptor influence on DA phasic signals. *A1*: somatodendritic DA levels during bursts (Δt_{burst} = 0.1 s, 0.3 s, and 0.6 s). *B1*: concurrent ν_{eff}. *Inset*: close view of firing rates. *C1*: DA levels in nucleus accumbens (NAcc). *D1*: activation of low-affinity receptors (DRL) during bursts. *E1*: activation of high-affinity receptors (DRH) during bursts. *Inset*: schematic illustration of positive (dark gray) and negative (light gray) contributions to the change in area under the curve (ΔAUC). *F1*: ΔAUC of DRL activity from bursts of duration Δt_{burst}. Circles, total ΔAUC including positive and negative contributions; asterisk, positive part of the peak only. *G1*: ΔAUC of DRH from bursts; same symbols as in *F1*. *A2*: somatodendritic DA levels during pauses (Δt_{pause} = 0.8 s, 1.6 s, 2.4 s). *B2*: ν_{eff} during and after the pauses. *C2*: DA levels in NAcc. *D2*: activation of DRL during pauses. *E2*: activation of DRH during pauses. *F2*: ΔAUC of DRL activity during pauses. Circles, negative contribution only; asterisk, total AUC including positive compensation by autoreceptors. *G2*: ΔAUC of DRH for pauses; same symbols as in *F2*.

The opposite effect was observed for pauses in firing patterns. Here there was a transient decrease in somatodendritic DA levels (Fig. 4*A2*) and subsequent increase up to 4.9 Hz in tonic firing rate (Fig. 4*B2*). In both cases the autoreceptor compensation increased with the duration of the phasic signal.

Phasic DA levels in NAcc were affected by compensation of somatodendritic and terminal autoreceptors. The bursts generated 0.2–0.4 μM DA transients in NAcc (Fig. 4*C1*). The combination of somatodendritic and presynaptic autoinhibition affected the shape of the transients, especially from long bursts. Thus after the transient DA levels in NAcc were reduced compared with tonic levels (Fig. 4*C1*) and after pauses DA levels were temporarily increased (Fig. 4*C2*).

We then evaluated the effect of bursts and pauses on time-resolved activity of DRH and DRL. With tonic firing of DA neurons, DRL were 6% activated. Bursts transiently increased activation to 20–30% depending on burst length (Fig. 4*D1*). Tonic firing led to 83% activation of DRH. Here bursts transiently increased activation to 90–95% depending on burst length (Fig. 4*E1*).

Autoreceptors dynamically affected activation of postsynaptic receptors after the bursts. Under some circumstances these effects contributed with nearly equal magnitude as the phasic signal itself (Fig. 4*E1*, *inset*). We therefore quantified the impact of the burst on postsynaptic DA receptors by calculating the ΔAUC of the receptor activation relative to the tonic baseline (*Eq. 10*). Upward transient receptor activation above baseline gives a positive contribution to the AUC; downward transients gives a negative contribution. In our case a burst first gave a transient of high activation, contributing positively to the AUC (see, for example, Fig. 4*E1*, *inset*). Bursts were followed by a period of lower than average receptor activity that gave a negative contribution to the AUC (see, for example, Fig. 4 *E1*, *inset*).

For low-affinity receptors, the net ΔAUC of the burst and subsequent autoreceptor inhibition was positive even though autoreceptors reduced the postsynaptic signal (Fig. 4*F1*).

On the other hand, the cancellation between positive and negative contributions to the ΔAUC was strong for DRH: Here the ΔAUC of the whole transient after the burst was nearly 0 (Fig. 4*G1*), whereas the positive contribution was of similar magnitude as the influence of bursts on DRL (Fig. 4*F1*). This indicates that autoreceptors strongly reduce the effect of isolated bursts when integrated by high-affinity receptors.

For pauses there was a similar trend: Here the autoreceptor contribution was positive and competed with the negative AUC generated by the pause. Effectively, autoreceptors gave a 30% reduction in DRL signaling of pauses; on the other hand, for DRH the compensation for pauses was hardly noticeable (Fig. 4, *F2* and *G2*).

Thus our model predicts that bursts affected the activation of low-affinity receptors more than high-affinity receptors (compare Fig. 4, *D1* and *E1*). Pauses in DA cell firing affected DRH more than DRL (compare Fig. 4, *D2* and *E2*). Autoreceptors increase the specificity in bursts and pauses targeting low- and high-affinity receptor populations.

Effect of DA uptake inhibition on dopamine signaling. The baseline level of extracellular DA in terminal and somatodendritic regions is sensitive to DA uptake inhibition. However, changes in uptake also evoke multiple compensatory responses of autoreceptors (Aragona et al. 2008; Einhorn et al. 1988; Rouge-Pont et al. 2002). The multiple competing effects make it difficult to deduce how DA uptake inhibitors affect DA signaling without the unified perspective on DA signaling offered by our model.

We first asked how different degrees of DA uptake inhibition would affect basal DA levels in NAcc.

In our model the coupling between somatodendritic DA levels and effective firing rate was deduced from experimental observations of firing rate as a function of cocaine dose. Therefore, the modeled reductions in firing rate induced by uptake inhibition will by definition be in agreement with experimental data from Einhorn et al. [compare Fig. 5*A1* with Fig. 1*A* (Einhorn et al. 1988)].

However, even though the firing rate was reduced, uptake inhibition increased the extracellular DA baseline in terminal regions of NAcc from 0.066 μM in the absence of uptake inhibition (K_{app} = 0.16 μM) to 0.134 μM with uptake inhibition equivalent to 15 mg/kg ip cocaine (K_{app} = 1.0 μM) (Fig. 5, *B1* and *E1*).

DA uptake inhibition affected tonic activation of postsynaptic receptors. For DRL, the activation increased almost proportionally with increased DA levels (Fig. 5, *C1* and *E1*). On the other hand the change in activation of DRH was minor (Fig. 5, *D1* and *E1*)

We then asked how DA uptake inhibition would affect postsynaptic signaling when tonic firing was interrupted by a burst (Fig. 5, *center*).

The duration of the burst was 0.25 s, equivalent to 5 spikes at 20-Hz effective firing rate (Grace and Bunney 1984a). The firing rate during bursts was only slightly affected by DA uptake inhibition (Fig. 5*A2*). Bursts transiently increased the concentration of extracellular DA in NAcc. Without uptake inhibition the height of the transient was 0.23 μM (Fig. 5*B2*). As uptake inhibition increased, the relative transient height remained nearly constant.

The transient changes in DA level were closely replicated by the activation of DRL (Fig. 5*C2*). To take into account the fact that uptake inhibition decreased the amplitude of transients but increased their width, we quantified the AUC of the transients compared with the baseline (*Eq. 10*). Then the net activation of DRL from bursts increased slightly (Fig. 5*E2*).

The integration of bursts by high-affinity postsynaptic receptors (DRH) was only marginally affected by DA uptake inhibition: Already 90% activated by tonic DA levels, the activity remained high in all conditions and was barely affected by DA uptake inhibition (Fig. 5, *D2* and *E2*).

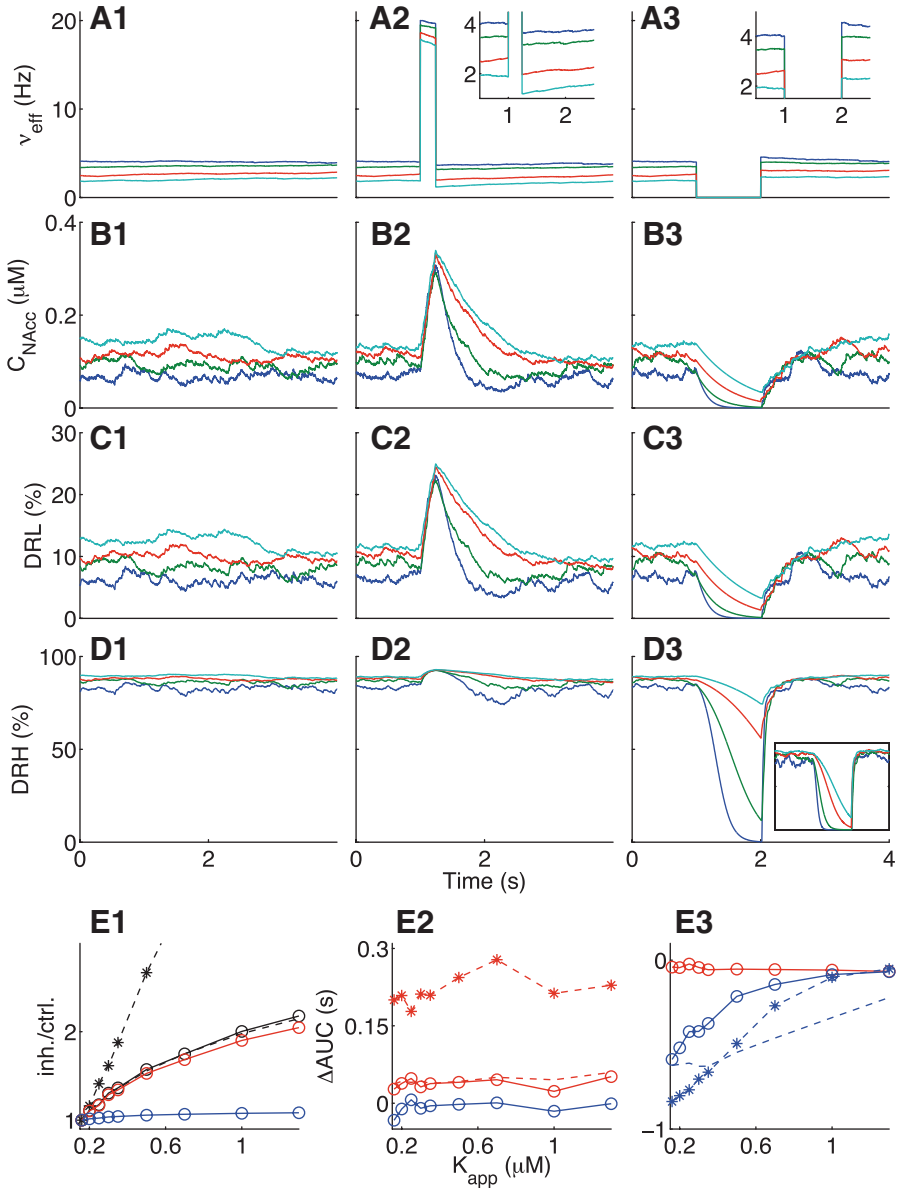

Fig. 5. Influence of DA uptake inhibition on the postsynaptic effect of phasic DA signaling. Except where noted the figure shows results for simulations of NAcc. Colors in *A–D* indicate different values of K_{app}. Blue, K_{app} = 0.16 μM (control); green, K_{app} = 0.35 μM; red, K_{app} = 0.7 μM; cyan, K_{app} = 1 μM. *A1–E1* show the effect of uptake inhibition on tonic firing. *A2–E2* show a burst (Δt_{burst} = 0.25 s). *A3–E3* show the effect of a pause (Δt_{pause} = 1 s). *A1–A3* show effective firing rate as function of time. *Insets* in *A2* and *A3* show close view of firing rate around the burst/pause. *B1–B3* show space-averaged DA levels, *C1–C3* show DRL activation, and *D1–D3* show DRH activation. *Inset* in *D3*: activation of DS DRH during pauses. Color code for *E1–E3*: black, DA levels; red, DRL; blue, DRH. Line styles in *E1–E3*: solid lines with circles, NAcc signals; dashed lines, DS signals; dashed with asterisks: autoreceptor knockout simulations. *E1*: relative increase in tonic signaling (inh/cntl) as function of K_{app}. *E2*: ΔAUC from bursts. *E3*: ΔAUC from pauses.

We then examined the effect of uptake inhibition on postsynaptic integration of a collective 1-s pause in DA cell firing.

As DA uptake inhibition only affected the tonic firing rate, the effective firing rate during the pause was always 0 (Fig. 5*A3* and *inset*).

In the absence of uptake inhibition the extracellular DA in NAcc was evacuated within a few hundred milliseconds of the onset of the pause (Fig. 5*B3*; see also Fig. 4). The lowest DA level during the pause was <1 nM.

With low levels of uptake inhibition, the time course of the temporal depletion of DA during the pause was only slightly changed and the lowest DA level was 3 nM (Fig. 5*B3*). With the highest level of DAT inhibition, the DA level remained above 50 nM despite the pause in cell firing (Fig. 5*B3*).

As before, activation of low-affinity postsynaptic receptors was also sensitive to low DA level in terminal regions during the pause (Fig. 5*C3*). DAT inhibition had relatively little effect on the ΔAUC from the pause (Fig. 5*E3*). However, the ability of high-affinity postsynaptic receptors to respond to pauses in DA neuron firing was dramatically reduced by DAT inhibition: The occurrence of low receptor activation during the pause was strongly reduced even by low levels of uptake inhibition (Fig. 5*D3*), and it was completely extinguished at intermediate levels and above (Fig. 5*D3*; see also Fig. 5*E3*).

We then tested the effect of DA uptake inhibition on phasic signaling in DS. Here we found similar change in basal DA level and in transient integration by low-affinity receptors as in NAcc (Fig. 5*E1*, DS and NAcc are nearly coincident; Fig. 5*E2*). However, compared with NAcc, the integration of pauses by DS high-affinity receptors was substantially less affected by uptake inhibition. For values of $K_{app} < 0.35$ μM there was very little change in ΔAUC. For $K_{app} > 0.35$ μM, the response was slower and full saturation was not observed (Fig. 5*D3*, *inset*, and Fig. 5*E3*).

Interestingly, the value of K_{app} at which the DS high-affinity receptor ΔAUC is reduced by 50% corresponds to a dose of 15 mg/kg ip cocaine. This correlates with the range of doses that lead to increased locomotor activity in rodents (Thomsen and Caine 2011). In a recent study it was shown that mice with conditional knockout of DA autoreceptors have increased sensitivity for the locomotor-stimulating effects of cocaine (Bello et al. 2011). We therefore asked whether removal of autoreceptors would also lead to increased sensitivity to uptake inhibition in our model. In particular, we asked whether saturation of high-affinity receptors would occur at a lower level of uptake inhibition (removal of terminal autoreceptors was simulated by setting $P_{min} = 14\%$, and removal of somatodendritic autoreceptors was simulated by setting $\nu_{eff} = \nu_{in}$ regardless of somatodendritic DA levels; other parameters were set for simulation of DS).

We found that DA levels increased much more strongly with uptake inhibition in the absence of autoreceptors (Fig. 5*E1*). Also, bursts gave terminal DA transients of the order of 1 μM. The ΔAUC for low-affinity receptors increased initially with uptake inhibition but was ultimately limited by saturation of the receptors (Fig. 5*E2*).

Importantly, high-affinity receptors were less sensitive to pauses under uptake inhibition: A reduction of 50% of the AUC occurred with $K_{app} = 0.55$ μM, equivalent to 6.9 mg/kg ip cocaine in agreement with experiment (Bello et al. 2011) (Fig. 5*E3*). It should be noted that in the absence of uptake inhibition the ΔAUC of the pause is slightly more negative in autoreceptor knockout simulations than simulations of normal DS. This is because of increased DA levels in autoreceptor knockout simulation giving higher tonic activation of the receptor before and after the pause.

Our estimates of P_{min} and P_{max} are subject to some experimental uncertainty, and biological variability in these variables is also expected. We therefore controlled for the sensitivity for details in our implementation by using a fixed-amplitude model to predict postsynaptic receptor activity (Dreyer et al. 2010). Here we found qualitatively similar results regarding the effect of DA inhibition on activation of postsynaptic receptors.

DISCUSSION

The model we present here involves a number of simplifications. For example, we did not include facilitation of DA release during burst firing (Montague et al. 2004). The effect of this assumption is apparent in our pair pulse study on short timescales where predictions of our model are lower compared with the in vivo observations (Fig. 3*A2*, $\Delta t < 0.1$ s) (Benoit-Marand et al. 2001). Also, since the aim of this study was to describe fast-timescale modulation by autoreceptors we did not take into account limited DA stores and autoreceptor regulation of the DA synthesis (Beaulieu and Gainetdinov 2011).

We described autoreceptors from a systems-level perspective. In this spirit we connected the occupancy of presynaptic autoreceptors directly to the terminal release probability and firing rate, omitting calculation of ionic currents mediated by GIRK channels associated with autoreceptors. The finite on- and off-rates of DA with autoreceptors were included for terminal autoreceptors only. This implicitly assumes that the interaction between DA and somatodendritic autoreceptors is much faster than variations in somatodendritic DA concentration (Beckstead et al. 2004; John et al. 2006).

In our study, DA uptake inhibition increased the basal DA level monotonically but not linearly (Fig. 5*E1*). In comparison, a meta-analysis of microdialysis studies by Frank et al. (2008) revealed a linear correlation between relative increase in basal DA level and ip administered dose of cocaine in milligrams per kilogram (Frank et al. 2008). At low or moderate doses our model agrees relatively well with the analysis by Frank et al.: For $K_{app} < 0.5$ μM (equivalent to ip cocaine <6 mg/kg) our model predicts increase tonic DA levels that agree by >80% of the result by Frank et al. However, at uptake inhibition equivalent to 20 mg/kg cocaine our model predicts only half the increase observed by Frank et al. In this respect it is also worth noting that we determined the somatodendritic influence on firing rates from empirical data of animals under anesthesia (Einhorn et al. 1988), where cocaine reduces the firing rate to a greater extent than recently observed in freely moving animals (Koulchitsky et al. 2012). We believe this could lead to our model underestimating the increase of DA by high doses of cocaine.

Our model of somatodendritic DA levels (*Eq. 4*) is based on voltammetry data from mouse slices (John et al. 2006). We found somatodendritic DA transients on the order of 100 nM, which is in relatively good agreement with other voltammetry observations in anesthetized rats (Kita et al. 2009) and in guinea pig slices (Rice et al. 1997). On the other hand, our

calculated tonic somatodendritic DA levels are higher than the 1 nM level reported with microdialysis (Kalivas and Duffy 1993). However, calculation of absolute DA levels from microdialysis measurements is a complex problem. Elaborate models suggest that tissue damage near dialysis probes influences measurements of basal DA levels (Borland et al. 2005; Bungay et al. 2003). Our model, on the other hand, is based on a minimal number of experimentally determined assumptions and does not take such effects into account. We therefore choose to test our model by predicting dynamical aspects of DA signaling where experimental data are less subject to such artifacts (Peters et al. 2004).

To our knowledge, the present model constitutes the first integrated description of DA signaling and how this is affected by both terminal and somatodendritic DA autoreceptors and DA uptake inhibition. Our analyses revealed a multitude of experimentally relevant dynamical effects of the dual autoreceptor system. We predict that somatodendritic autoinhibition exerts indirect influence on terminal release: Strong evoked release induced a reduction of tonic cell firing that led to facilitation of terminal release 3–8 s after the transient (Fig. 3*E*). Even though the compensatory effects of autoreceptors are appreciable, they do not invalidate our previous estimates of the postsynaptic response to phasic reward related signals (Dreyer et al. 2010): Low-affinity receptors were sensitive to bursts, and high-affinity receptors were mostly sensitive to pauses (Fig. 4, *F1* and *G2*). Autoreceptors strongly compensated the effect of bursts on high-affinity receptors and also reduced the effect of pauses on low-affinity receptors, which increases selectivity of bursts and pauses in targeting different receptor populations (Fig. 4, *G1* and *F1*).

We applied the model to the case of DA uptake inhibition and investigated how this would affect postsynaptic integration of tonic and phasic DA signals. Our model was in agreement with experimental studies suggesting a strong influence of DA autoreceptors in the effect of cocaine (Aragona et al. 2008; Bello et al. 2011; Rouge-Pont et al. 2002).

The most prominent postsynaptic effect of uptake inhibition was that DRH decoupled from pauses in phasic firing patters (Fig. 5*C*). At certain levels of uptake inhibition DRH receptor signaling underwent a transition from phasic (DRH activation sensitive to pauses in firing pattern) to essentially tonic (DRH tonically activated regardless of firing pattern). In NAcc high-affinity receptor decoupling occurred at therapeutic levels of uptake inhibition, similar to 2.7 mg/kg ip MP. In DS the same degree of decoupling occurred with uptake inhibition close to locomotor-stimulating doses of ~15 mg/kg ip cocaine (Thomsen and Caine 2011). Removal of autoreceptor control led to decoupling at lower levels of uptake inhibition, similar to 7 mg/kg ip cocaine.

Obviously the exact location of the transition from phasic to tonic activation of DRH is depending on our choice of 1 s as a "typical" length of a pause in DAergic firing. We also tested high- and low-affinity receptor activation with a phasic firing pattern containing a distribution of bursts and pauses of different length. Here short pauses were decoupled at even lower levels of uptake inhibition, while postsynaptic integration of long pauses was reliable at higher levels of uptake inhibition and with similar differences between NAcc and DS (not shown). Pauses in DA cell firing observed in classical reward prediction experiments are on the order of 200–400 ms (Bayer et al. 2007; Schultz 1998). However, in other experimental paradigms the inhibition of DA neuronal activity may last several seconds (Mileykovskiy and Morales 2011), and 1-s pauses in firing are relatively common in phasic firing patterns (see examples in Bingmer et al. 2011).

DA D1-like and D2-like receptors have both high-affinity and low-affinity states for agonist binding (May 1992). However, indisputable determination of the biological function of these states is still lacking (Skinbjerg et al. 2012). Our implementation of autoreceptors embraces this range of affinities: The high somatodendritic DA levels required to reduce effective firing rate implicitly assume low affinity of somatodendritic D2 autoreceptors, whereas our presynaptic D2 autoreceptors are assumed to have $EC_{50} \approx 40$ nM.

Assuming that postsynaptic D2 receptors are predominantly in the high-affinity state and that D1 receptors are in the low-affinity state, our model complies with in vivo studies showing high tonic activity of D2 receptors (Bertran-Gonzalez et al. 2008; Svenningsson et al. 2000). However, this raises new questions because D2 receptors are often ascribed an important role in mediating hyperlocomotor effects of DA uptake inhibitors (Chausmer and Katz 2001). How can this be possible if they are already saturated by spontaneous DAergic activity? We resolve this problem by considering high-affinity D2 receptors to be modulated by a dynamic DA signal. In the unperturbed state, pauses in DA cell firing constitute an efficient method for mediating time-resolved signals to high-affinity receptors. However, this signal is crucially dependent on DAT to remove extracellular DA during the pause. Therefore low and intermediate doses of DA uptake strongly modulate or even block this part of the DA signal with sensitivity inversely dependent on V_{max}.

Under the hypothesis that DRH describes the majority of D2 receptors and DRL describes D1 receptors, our model predicts that DA uptake inhibitors will influence postsynaptic targets differently depending on the activity state of DA neurons. With tonically firing DA neurons DAT inhibitors mainly increase D1 receptor activation but leave D2 activation largely unaffected (Fig. 5*E1*). This is similar to observations by Svenningson et al. (2000) and by Bertran-Gonzalez et al. (2008). However, with phasically firing DA neurons, where firing patterns include bursts and pauses, both D1 and D2 signaling are affected. As a corollary, our model predicts that in experimental paradigms associated with increased phasic signaling, such as stress (Anstrom et al. 2009; Valenti et al. 2011), locomotor responses to DA uptake inhibition will be augmented compared with experimental situations in which DA signal is dominated by tonic firing.

The exact role of DA in the therapeutic mechanism of psychostimulant medication of ADHD is debated (Gonon 2009; Volkow et al. 2011). Even though the present results suggest that significant changes in high-affinity receptor signaling can occur at therapeutic doses, this does not exclude that other mechanisms, such as norepinephrine or DA signaling in prefrontal cortex, mediate the therapeutically beneficial action of MP in ADHD (Berridge et al. 2006). Thus it may as well be that the changes in phasic DA signaling we observe are an adverse effect and that the therapeutically optimal dose has minimal influence.

In summary, our mathematical model provides a unified description of the link between somatodendritic DA release,

firing patterns of DA neurons, and pre- and postsynaptic DA receptor activation. We used this model to show that the qualitative effect of DAT inhibition depends strongly on the firing patterns of DA neurons and identified critical levels of uptake inhibition at which high-affinity DA receptor signaling loses sensitivity to pauses in DA cell firing. In NAcc this effect occurred in the therapeutic range of DAT inhibition, whereas high-affinity receptors in DS were sensitive to higher levels that induce locomotor symptoms in behaving animals.

GRANTS

J. K. Dreyer is supported by the Lundbeck Foundation (Grant No. R77-A6926).

DISCLOSURES

No conflicts of interest, financial or otherwise, are declared by the author(s).

AUTHOR CONTRIBUTIONS

Author contributions: J.K.D. conception and design of research; J.K.D. performed experiments; J.K.D. and J.H. analyzed data; J.K.D. and J.H. interpreted results of experiments; J.K.D. prepared figures; J.K.D. drafted manuscript; J.K.D. and J.H. edited and revised manuscript; J.K.D. and J.H. approved final version of manuscript.

REFERENCES

Anstrom KK, Miczek KA, Budygin EA. Increased phasic dopamine signaling in the mesolimbic pathway during social defeat in rats. *Neuroscience* 161: 3–12, 2009.

Aragona BJ, Cleaveland NA, Stuber GD, Day JJ, Carelli RM, Wightman RM. Preferential enhancement of dopamine transmission within the nucleus accumbens shell by cocaine is attributable to a direct increase in phasic dopamine release events. *J Neurosci* 28: 8821–8831, 2008.

Bayer HM, Lau B, Glimcher PW. Statistics of midbrain dopamine neuron spike trains in the awake primate. *J Neurophysiol* 98: 1428–1439, 2007.

Beaulieu JM, Gainetdinov RR. The physiology, signaling, and pharmacology of dopamine receptors. *Pharmacol Rev* 63: 182–217, 2011.

Beckstead MJ, Grandy DK, Wickman K, Williams JT. Vesicular dopamine release elicits an inhibitory postsynaptic current in midbrain dopamine neurons. *Neuron* 42: 939–946, 2004.

Bello EP, Mateo Y, Gelman DM, Noain D, Shin JH, Low MJ, Alvarez VA, Lovinger DM, Rubinstein M. Cocaine supersensitivity and enhanced motivation for reward in mice lacking dopamine D2 autoreceptors. *Nat Neurosci* 14: 1033–1038, 2011.

Benoit-Marand M, Borrelli E, Gonon F. Inhibition of dopamine release via presynaptic D2 receptors: time course and functional characteristics in vivo. *J Neurosci* 21: 9134–9141, 2001.

Berridge CW, Devilbiss DM, Andrzejewski ME, Arnsten AF, Kelley AE, Schmeichel B, Hamilton C, Spencer RC. Methylphenidate preferentially increases catecholamine neurotransmission within the prefrontal cortex at low doses that enhance cognitive function. *Biol Psychiatry* 60: 1111–1120, 2006.

Bertran-Gonzalez J, Bosch C, Maroteaux M, Matamales M, Herve D, Valjent E, Girault JA. Opposing patterns of signaling activation in dopamine D1 and D2 receptor-expressing striatal neurons in response to cocaine and haloperidol. *J Neurosci* 28: 5671–5685, 2008.

Bingmer M, Schiemann J, Roeper J, Schneider G. Measuring burstiness and regularity in oscillatory spike trains. *J Neurosci Methods* 201: 426–437, 2011.

Borland LM, Shi G, Yang H, Michael AC. Voltammetric study of extracellular dopamine near microdialysis probes acutely implanted in the striatum of the anesthetized rat. *J Neurosci Methods* 146: 149–158, 2005.

Buckholtz JW, Treadway MT, Cowan RL, Woodward ND, Li R, Ansari MS, Baldwin RM, Schwartzman AN, Shelby ES, Smith CE, Kessler RM, Zald DH. Dopaminergic network differences in human impulsivity. *Science* 329: 532, 2010.

Bungay PM, Newton-Vinson P, Isele W, Garris PA, Justice JB. Microdialysis of dopamine interpreted with quantitative model incorporating probe implantation trauma. *J Neurochem* 86: 932–946, 2003.

Chance B. The kinetics of the enzyme-substrate compound of peroxidase. *J Biol Chem* 151: 553–577, 1943.

Chausmer AL, Katz JL. The role of D2-like dopamine receptors in the locomotor stimulant effects of cocaine in mice. *Psychopharmacology (Berl)* 155: 69–77, 2001.

Cools R, D'Esposito M. Inverted-U-shaped dopamine actions on human working memory and cognitive control. *Biol Psychiatry* 69: e113–e125, 2011.

Cragg SJ, Greenfield SA. Differential autoreceptor control of somatodendritic and axon terminal dopamine release in substantia nigra, ventral tegmental area, and striatum. *J Neurosci* 17: 5738–5746, 1997.

Cragg SJ, Rice ME. DAncing past the DAT at a DA synapse. *Trends Neurosci* 27: 270–277, 2004.

Dagher A, Robbins TW. Personality, addiction, dopamine: insights from Parkinson's disease. *Neuron* 61: 502–510, 2009.

Doucet G, Descarries L, Garcia S. Quantification of the dopamine innervation in adult rat neostriatum. *Neuroscience* 19: 427–445, 1986.

Dreyer JK, Herrik KF, Berg RW, Hounsgaard JD. Influence of phasic and tonic dopamine release on receptor activation. *J Neurosci* 30: 14273–14283, 2010.

Dugast C, Brun P, Sotty F, Renaud B, Suaud-Chagny MF. On the involvement of a tonic dopamine D2-autoinhibition in the regulation of pulse-to-pulse-evoked dopamine release in the rat striatum in vivo. *Naunyn Schmiedebergs Arch Pharmacol* 355: 716–719, 1997.

Einhorn LC, Johansen PA, White FJ. Electrophysiological effects of cocaine in the mesoaccumbens dopamine system: studies in the ventral tegmental area. *J Neurosci* 8: 100–112, 1988.

el Mestikawy S, Glowinski J, Hamon M. Presynaptic dopamine autoreceptors control tyrosine hydroxylase activation in depolarized striatal dopaminergic terminals. *J Neurochem* 46: 12–22, 1986.

Espana RA, Roberts DC, Jones SR. Short-acting cocaine and long-acting GBR-12909 both elicit rapid dopamine uptake inhibition following intravenous delivery. *Neuroscience* 155: 250–257, 2008.

Frank ST, Krumm B, Spanagel R. Cocaine-induced dopamine overflow within the nucleus accumbens measured by in vivo microdialysis: a meta-analysis. *Synapse* 62: 243–252, 2008.

Garris PA, Ciolkowski EL, Pastore P, Wightman RM. Efflux of dopamine from the synaptic cleft in the nucleus accumbens of the rat brain. *J Neurosci* 14: 6084–6093, 1994a.

Garris PA, Ciolkowski EL, Wightman RM. Heterogeneity of evoked dopamine overflow within the striatal and striatoamygdaloid regions. *Neuroscience* 59: 417–427, 1994b.

Gonon F. The dopaminergic hypothesis of attention-deficit/hyperactivity disorder needs re-examining. *Trends Neurosci* 32: 2–8, 2009.

Gonon FG, Buda MJ. Regulation of dopamine release by impulse flow and by autoreceptors as studied by in vivo voltammetry in the rat striatum. *Neuroscience* 14: 765–774, 1985.

Grace AA, Bunney BS. The control of firing pattern in nigral dopamine neurons: burst firing. *J Neurosci* 4: 2877–2890, 1984a.

Grace AA, Bunney BS. The control of firing pattern in nigral dopamine neurons: single spike firing. *J Neurosci* 4: 2866–2876, 1984b.

Grace AA, Floresco SB, Goto Y, Lodge DJ. Regulation of firing of dopaminergic neurons and control of goal-directed behaviors. *Trends Neurosci* 30: 220–227, 2007.

Herr NR, Daniel KB, Belle AM, Carelli RM, Wightman RM. Probing presynaptic regulation of extracellular dopamine with iontophoresis. *ACS Chem Neurosci* 1: 627–638, 2010.

Hersch SM, Yi H, Heilman CJ, Edwards RH, Levey AI. Subcellular localization and molecular topology of the dopamine transporter in the striatum and substantia nigra. *J Comp Neurol* 388: 211–227, 1997.

Howes OD, Kapur S. The dopamine hypothesis of schizophrenia: version III—the final common pathway. *Schizophr Bull* 35: 549–562, 2009.

Hyland BI, Reynolds JN, Hay J, Perk CG, Miller R. Firing modes of midbrain dopamine cells in the freely moving rat. *Neuroscience* 114: 475–492, 2002.

John CE, Budygin EA, Mateo Y, Jones SR. Neurochemical characterization of the release and uptake of dopamine in ventral tegmental area and serotonin in substantia nigra of the mouse. *J Neurochem* 96: 267–282, 2006.

John CE, Jones SR. Voltammetric characterization of the effect of monoamine uptake inhibitors and releasers on dopamine and serotonin uptake in

mouse caudate-putamen and substantia nigra slices. *Neuropharmacology* 52: 1596–1605, 2007.

Kalivas PW, Duffy P. Time course of extracellular dopamine and behavioral sensitization to cocaine. II. Dopamine perikarya. *J Neurosci* 13: 276–284, 1993.

Kita JM, Kile BM, Parker LE, Wightman RM. In vivo measurement of somatodendritic release of dopamine in the ventral tegmental area. *Synapse* 63: 951–960, 2009.

Koulchitsky S, De Backer B, Quertemont E, Charlier C, Seutin V. Differential effects of cocaine on dopamine neuron firing in awake and anesthetized rats. *Neuropsychopharmacology* 37: 1559–1571, 2012.

Kuhr WG, Wightman RM, Rebec GV. Dopaminergic neurons: simultaneous measurements of dopamine release and single-unit activity during stimulation of the medial forebrain bundle. *Brain Res* 418: 122–128, 1987.

May T. Striatal dopamine D1-like receptors have higher affinity for dopamine in ethanol-treated rats. *Eur J Pharmacol* 215: 313–316, 1992.

Mileykovskiy B, Morales M. Duration of inhibition of ventral tegmental area dopamine neurons encodes a level of conditioned fear. *J Neurosci* 31: 7471–7476, 2011.

Moller HJ. Antipsychotic and antidepressive effects of second generation antipsychotics: two different pharmacological mechanisms? *Eur Arch Psychiatry Clin Neurosci* 255: 190–201, 2005.

Montague PR, McClure SM, Baldwin PR, Phillips PE, Budygin EA, Stuber GD, Kilpatrick MR, Wightman RM. Dynamic gain control of dopamine delivery in freely moving animals. *J Neurosci* 24: 1754–1759, 2004.

Moquin KF, Michael AC. Tonic autoinhibition contributes to the heterogeneity of evoked dopamine release in the rat striatum. *J Neurochem* 110: 1491–1501, 2009.

Oleson EB, Salek J, Bonin KD, Jones SR, Budygin EA. Real-time voltammetric detection of cocaine-induced dopamine changes in the striatum of freely moving mice. *Neurosci Lett* 467: 144–146, 2009.

Peters JL, Miner LH, Michael AC, Sesack SR. Ultrastructure at carbon fiber microelectrode implantation sites after acute voltammetric measurements in the striatum of anesthetized rats. *J Neurosci Methods* 137: 9–23, 2004.

Phillips PE, Hancock PJ, Stamford JA. Time window of autoreceptor-mediated inhibition of limbic and striatal dopamine release. *Synapse* 44: 15–22, 2002.

Pickel VM, Johnson E, Carson M, Chan J. Ultrastructure of spared dopamine terminals in caudate-putamen nuclei of adult rats neonatally treated with intranigral 6-hydroxydopamine. *Brain Res Dev Brain Res* 70: 75–86, 1992.

Pucak ML, Grace AA. Evidence that systemically administered dopamine antagonists activate dopamine neuron firing primarily by blockade of somatodendritic autoreceptors. *J Pharmacol Exp Therapeut* 271: 1181–1192, 1994.

Rice ME, Cragg SJ, Greenfield SA. Characteristics of electrically evoked somatodendritic dopamine release in substantia nigra and ventral tegmental area in vitro. *J Neurophysiol* 77: 853–862, 1997.

Rouge-Pont F, Usiello A, Benoit-Marand M, Gonon F, Piazza PV, Borrelli E. Changes in extracellular dopamine induced by morphine and cocaine: crucial control by D2 receptors. *J Neurosci* 22: 3293–3301, 2002.

Schmitz Y, Benoit-Marand M, Gonon F, Sulzer D. Presynaptic regulation of dopaminergic neurotransmission. *J Neurochem* 87: 273–289, 2003.

Schultz W. Predictive reward signal of dopamine neurons. *J Neurophysiol* 80: 1–27, 1998.

Skinbjerg M, Sibley DR, Javitch JA, Abi-Dargham A. Imaging the high-affinity state of the dopamine D2 receptor in vivo: fact or fiction? *Biochem Pharmacol* 83: 193–198, 2012.

Svenningsson P, Lindskog M, Ledent C, Parmentier M, Greengard P, Fredholm BB, Fisone G. Regulation of the phosphorylation of the dopamine- and cAMP-regulated phosphoprotein of 32 kDa in vivo by dopamine D1, dopamine D2, and adenosine A2A receptors. *Proc Natl Acad Sci USA* 97: 1856–1860, 2000.

Thomsen M, Caine SB. Psychomotor stimulant effects of cocaine in rats and 15 mouse strains. *Exp Clin Psychopharmacol* 19: 321–341, 2011.

Valenti O, Lodge DJ, Grace AA. Aversive stimuli alter ventral tegmental area dopamine neuron activity via a common action in the ventral hippocampus. *J Neurosci* 31: 4280–4289, 2011.

Venton BJ, Zhang H, Garris PA, Phillips PE, Sulzer D, Wightman RM. Real-time decoding of dopamine concentration changes in the caudate-putamen during tonic and phasic firing. *J Neurochem* 87: 1284–1295, 2003.

Volkow ND, Wang GJ, Fowler JS, Gatley SJ, Logan J, Ding YS, Hitzemann R, Pappas N. Dopamine transporter occupancies in the human brain induced by therapeutic doses of oral methylphenidate. *Am J Psychiatry* 155: 1325–1331, 1998.

Volkow ND, Wang GJ, Newcorn JH, Kollins SH, Wigal TL, Telang F, Fowler JS, Goldstein RZ, Klein N, Logan J, Wong C, Swanson JM. Motivation deficit in ADHD is associated with dysfunction of the dopamine reward pathway. *Mol Psychiatry* 16: 1147–1154, 2011.

Wallace LJ, Hughes RM. Computational analysis of stimulated dopaminergic synapses suggests release largely occurs from a single pool of vesicles. *Synapse* 62: 909–919, 2008.

Wightman RM, Heien ML, Wassum KM, Sombers LA, Aragona BJ, Khan AS, Ariansen JL, Cheer JF, Phillips PE, Carelli RM. Dopamine release is heterogeneous within microenvironments of the rat nucleus accumbens. *Eur J Neurosci* 26: 2046–2054, 2007.

Wightman RM, Zimmerman JB. Control of dopamine extracellular concentration in rat striatum by impulse flow and uptake. *Brain Res Brain Res Rev* 15: 135–144, 1990.

Wu Q, Reith ME, Walker QD, Kuhn CM, Carroll FI, Garris PA. Concurrent autoreceptor-mediated control of dopamine release and uptake during neurotransmission: an in vivo voltammetric study. *J Neurosci* 22: 6272–6281, 2002.

Zhang L, Doyon WM, Clark JJ, Phillips PE, Dani JA. Controls of tonic and phasic dopamine transmission in the dorsal and ventral striatum. *Mol Pharmacol* 76: 396–404, 2009.